



HAL
open science

Study of hydrothermal aging impact on Na- and P-modified diesel oxidation catalyst (DOC)

P. Anguita, F. Gaillard, E. Iojoiu, S. Gil, A. Giroir-Fendler

► **To cite this version:**

P. Anguita, F. Gaillard, E. Iojoiu, S. Gil, A. Giroir-Fendler. Study of hydrothermal aging impact on Na- and P-modified diesel oxidation catalyst (DOC). *Journal of Catalysis*, 2019, 375 (—), pp.329-338. 10.1016/j.jcat.2019.06.028 . hal-02306747

HAL Id: hal-02306747

<https://hal.science/hal-02306747>

Submitted on 25 Oct 2021

HAL is a multi-disciplinary open access archive for the deposit and dissemination of scientific research documents, whether they are published or not. The documents may come from teaching and research institutions in France or abroad, or from public or private research centers.

L'archive ouverte pluridisciplinaire **HAL**, est destinée au dépôt et à la diffusion de documents scientifiques de niveau recherche, publiés ou non, émanant des établissements d'enseignement et de recherche français ou étrangers, des laboratoires publics ou privés.



Distributed under a Creative Commons Attribution - NonCommercial 4.0 International License

Study of hydrothermal aging impact on Na- and P-modified diesel oxidation catalyst (DOC)

Paola Anguita,^a François Gaillard,^a Eduard Iojoiu,^b Sonia Gil,^{a*} Anne Giroir-Fendler^{a*}

^aUniv Lyon, Université Lyon 1, CNRS, UMR 5256, IRCELYON, 2 avenue Albert Einstein, Villeurbanne, F-69622, France.

^bRenault Trucks - Volvo Group Trucks Technology, Powertrain Engineering, 99 route de Lyon – 69806 Saint-Priest Cedex, France

**Corresponding authors: anne.giroir-fendler@ircelyon.univ-lyon1.fr;
sonia.gil@ircelyon.univ-lyon1.fr*

Abstract

The effects of hydrothermal aging (HT-aging), of a biodiesel oxidation catalyst in presence of Na and P impurities were studied. The synthesized reference-PtPd/CeZrO₂/La-Al₂O₃ and Na-, P-modified-PtPd/CeZrO₂/La-Al₂O₃ catalysts were HT-aged, characterized by several techniques and catalytically tested. The characterization results showed the loss of specific surface area due to the sintering of the catalyst. H₂-TPR results evidenced the decrease of the catalytic redox activity. TEM results indicated that sodium impurities did not modified the catalyst structure while phosphates were formed. In general, lower reaction rates were found for CO, C₃H₆ and NO involved reactions after HT-aging. The electronic changes induced by sodium species were attenuated after HT-aging due to the sintering of the catalyst. The lower metal-adsorbates charge transfer enhanced CO oxidation while had a negative effect for C₃H₆ and NO involved reactions. Diffuse Reflectance Infrared Fourier Transform Spectroscopy experiments indicated that phosphates inhibited the intermediates adsorption on the catalyst surface.

Keywords: hydrothermal aging, sodium impurities, phosphorus species, diesel oxidation catalyst, DRIFTS.

1. Introduction

The legislation concerning the exhaust emissions of automobile is continuously tightened, requiring more active and durable catalysts. The last published normative EURO VI, requires a minimum durability of 700 000 km for heavy-duty vehicles [1]. Diesel Oxidation Catalysts (DOCs) are critical component of current diesel exhaust systems along with diesel particulate filters (DPF) and selective catalytic reduction catalysts (SCR) [2]. DOC could efficiently eliminate the CO, hydrocarbons and convert NO to NO₂, which plays a crucial role in the promotion of soot oxidation [3] and the low-temperature activity for SCR [4].

On the other hand, biodiesel has been depicted as a promising alternative fuel to conventional diesel due to the similar calorific power and the better carbon balance, which implies lower net emissions of CO₂. However, the use of biodiesel exposes the catalysts to kilograms of impurities, such as Na, coming from its liquid-phase synthesis. Alkali ions are known to modify the activity and selectivity of metal catalysts. Previous studies [5–7] have shown that electropositive promoters, such as alkali metals, enhanced the catalytic activity of supported Pt-group metal catalysts in the NO reduction rate, as well as the N₂ selectivity. These effects were associated with the electron donor behaviour of alkali metals, which would induce electronic changes on the metal catalysts. The addition of alkali metal ions to noble metal would increase the strength of the metal – electron-acceptor (eg. NO, CO) bonds. Our previous study [8] showed that the nature of alkali and the added amount could have different effects over catalytic activity of DOC reference catalysts. The results showed that the strengthening of CO and NO adsorptions in presence of Na impurities had a negative influence on the obtained reaction rates. Nevertheless, H₂-TPR results evidenced a higher interaction of the catalyst with the oxygen in presence of Na impurities that enhanced the propylene oxidation.

In addition, phosphorus species derived from the anti-wear component ZDDP (zinc dialkyldithiophosphate) commonly present in engine oils could also have an important influence on performance of DOC catalysts [9]. These species could produce the catalyst pore sites blockage and modify the composition of the support [10]. In our previous study [8], we have verified that the addition of phosphorus to the catalyst leads changes on the catalytic activity of DOC. The high amount of phosphorus incorporated to the catalyst produced the formation of phosphates, which could block the catalytic active sites. Thus, the CO and C₃H₆ reaction rates were

enhanced due to the inhibition of the “self-poisoning” effect produced by saturation of the catalyst surface. However, as verified by NO-TPD the NO adsorption was diminished, and so the NO oxidation was disfavored.

Additionally to the effects produced by the impurities coming from the biodiesel use, the stability of DOC catalysts become questionable when it is exposed at temperatures higher than 600 °C. Related to the configuration used in heavy-duty after-treatment systems, in which DOC is placed next to DPF, the former often experience very high temperatures, i.e. during active regeneration of DPF [11]. In particular, platinum metal particles that are traditionally used on DOC formulations due to its high activity for NO oxidation, sinter by Ostwald ripening mechanism at high temperatures under oxidation conditions, involving metal particles growth by coalescence [12,13]. This sinter of the catalyst could produce the thermal deactivation of DOC, decreasing its catalytic activity. Thus, the Pt is usually combined with Pd in order to avoid Pt sintering. Earlier studies have demonstrated a synergetic effect in terms of thermal stability during interaction of Pt with Pd [14–16]. It has been verified that Pt-Pd bimetallic particles sinter more slowly than pure Pt does, which is related to the inhibition of Pt volatilization due to the low vapour pressure of Pd [17]. Although the use of Pt-Pd bimetallic catalysts delays the sintering process, previous studies have shown a loss of redox properties [18,19]. Otherwise, alkali metals affect the thermal properties of the support and can accelerate the sintering process, i.e. by interaction with acid sites of the alumina [20]. In addition, previous studies have demonstrated that the combination of phosphorus impurities with high temperatures has a strong effect on the activity of Pt-based catalysts [21].

Thus, DOC can be deactivated by chemical mechanisms, due to the accumulation of contaminants that can act as poisons on the active surface of the catalyst, and by thermal mechanisms due to the high temperatures experienced during DPF active regeneration. However, a clear description for the combined effects of high temperatures and impurities coming from biodiesel and automotive lubricants is still unclear. The goal of the present study is to verify the stability upon hydrothermal aging conditions of a DOC model catalyst, PtPd/CeZrO₂/La-Al₂O₃, in presence of Na and P impurities. Characterization by N₂ adsorption/desorption, XRD, TEM, XPS and H₂-TPR of hydrothermally aged samples provided insight of morphological changes of the catalysts. The catalytic performance in operating conditions of hydrothermally aged catalysts was addressed and compared with our previous results for the same

stabilized catalysts. In addition, DRIFT spectroscopy was used to get a deeper understanding about the reaction mechanisms.

2. Experimental

2.1. Catalysts preparation

Reference catalyst was obtained by successive impregnations of an alumina support obtained by calcination of γ -Al₂O₃ (Alfa Aesar) at 650 °C for 5h under air flow (50 ml min⁻¹) containing 10% water. The alumina was stabilized with 4 wt% of lanthanum also added by incipient wetness impregnation, using an aqueous solution of La(NO₃)₃·6H₂O (Sigma Aldrich). A complementary phase of ceria-zirconia (10 wt%, Ce/Zr weight ratio of 2.5) was added by co-impregnation of the lanthanum doped alumina with an aqueous solution of cerium (III) nitrate hexahydrate (Sigma Aldrich) and zirconyl nitrate hydrate (Sigma Aldrich) as precursors of cerium and zirconium, respectively. Finally, an aqueous solution of Pt(NH₃)₄(NO₃)₂ (Sigma Aldrich) and Pd(NO₃)₂ (Sigma Aldrich) was co-impregnated on the CeZrO₂/La-Al₂O₃ support, followed with the same calcination conditions. Thus, the obtained reference catalyst was composed of 0.71 wt% Pt – 0.47 wt% Pd/CeZrO₂/La-Al₂O₃. After that, the impurities were also added by incipient wetness impregnation method of aqueous solutions of NaNO₃ (Sigma Aldrich) or (NH₄)₂HPO₄ (Sigma Aldrich). The amount of impurities added was related to real percentage found on DOCs based on biodiesel fuel consumption of 35 L/km for a truck during 700 000 km. The modified catalysts synthesized were: 1.6 wt% Na- and 5.6 wt% P-PtPd/CeZrO₂/La-Al₂O₃ catalysts.

Once the reference and modified catalysts were synthesized, they were submitted to a hydrothermal aging protocol in order to study the influence of aging conditions. The stabilized catalysts were hydrothermally (HT) aged at 850 °C during 16 h under 10% water and 50 ml min⁻¹ of air flow.

2.2. Catalyst characterization

The chemical composition of the different catalysts was quantitatively determined using inductively coupled plasma optical emission spectroscopy (ICP-OES) on a flame Perkin Elmer M1100 spectrometer. Before the measurement, the metal oxides were dissolved using a mixture of inorganic acids (H₂SO₄, HNO₃ and

HF).

Powder X-ray diffraction (XRD) patterns of all catalysts were obtained using a Bruker D8 diffractometer (CuK α radiation at 0.154184 nm) equipped with a Ni filter and 1-D fast multistrip detector (LynxEye, 192 channels on 2.95°). The diffractograms were collected at 2 θ with steps of 0.02° from 4° to 80° for the total acquisition time of 32 min. Phase identification was carried out using the Diffrac.Eva software (Bruker) and the ICDD-PDF4+ database.

Nitrogen adsorption and desorption isotherms were measured at -196 °C on a Micromeritics ASAP 2020 surface area and porosity analyzer. Primary, the catalysts were degassed at 300 °C for 3 h under primary vacuum. The specific surface area of each catalyst was calculated from the linear part using the Brunauer-Emmett-Teller (BET) method ($P/P_0 = 0.05-0.25$). The porous volume and the pore size distribution were calculated using the Barrett-Joyner-Halenda (BJH) method.

Transmission electron microscopy (TEM) observations of the catalysts were performed on a JEM-2100 microscope with EDX detector. All catalysts were ultrasonically dispersed in ethanol and then dried over a copper grid coated with a carbon film.

X-ray photoelectron spectroscopy (XPS) analysis was carried out on a Kratos Analytical AXIS Ultra DLD electron spectrometer using the AlK α (1486.6 eV) radiation source. In order to compare all the spectra recorded, the Al2p peak from Al₂O₃ present in the catalysts was selected as a binding energy reference as no variations were detected, and its value fixed at 74.6 eV.

The reducibility of the catalysts was examined by hydrogen temperature programmed reduction (H₂-TPR) using mass spectrometer detection (Hiden, HPR 20). Prior to the test, the catalyst (about 100 mg) was firstly pre-treated at 600 °C for 15 min in a synthetic air flow of 50 ml min⁻¹ and then cooled down to room temperature in an air flow. It was followed by 5 minutes of purge in an Ar flow, controlled by residual O₂ analysis. 2% H₂/Ar with a flow rate of 50 ml min⁻¹ as the reducing gas was introduced and the reactor was heated from 25 to 650 °C with a rate of 20 °C min⁻¹. H₂ consumption was quantitatively calculated by time integration of H₂-TPR profiles. Concomitant H₂O evolution was also recorded.

2.3. Catalyst activity measurements

The catalytic behaviour was tested in a U tubular quartz reactor with the catalyst placed on a fritted quartz place (30 mm in length and 8 mm in internal diameter). The reactor was heated with a furnace and the temperature measured with a K-type thermocouple (Omega). The water content in the reaction mixture was controlled using the vapour pressure of H₂O at the temperature of the saturator (28 °C) controlled by a heating bath. All lines placed downstream from the saturator were heated above 100 °C to prevent condensation. Catalytic tests were carried out using 50 mg of catalysts and a reactant mixture containing [NO] \approx 500 ppm, [CO] \approx 300 ppm, [C₃H₆] \approx 300 ppm, [CO₂] \approx 5 vol.%, [O₂] \approx 10 vol.%, [H₂O] \approx 3.5 vol.% and He as the carrier gas, with the total flow of 250 ml min⁻¹. The gas hourly space velocity (GHSV) of the total gas mixture was fixed at 135000 h⁻¹. Temperature was increased and decreased by a ramp of 5 °C min⁻¹ from 80 °C up to 600 °C. Three consecutive temperature cycles were performed to analyse the catalytic stability. Gas effluents were analysed with a micro gas chromatograph (SRA % GC-R3000) and an infrared-ultraviolet spectroscopy (EMERSON IR/UV X-STREAM Enhanced XEGP).

2.4. DRIFT spectroscopy

In-situ DRIFT experiment were conducted by a Thermo Scientific Nicolet iS50 spectrometer equipped with a MCT detector and heated reaction cell with KBr windows (Harrick Scientific, Praying Mantis) in which the catalyst powder was placed. During spectra acquisition the external optics were purged with CO₂-free dry air generated from an air purifier system (Parker Balston, FT-IR purge gas generator). The DRIFTS spectra were collected in the 4000-650 cm⁻¹ wavenumber range, accumulating 98 scans at 4 cm⁻¹ resolutions. A Temperature Controller (ATC, Harrick Scientific) was connected to the chamber to monitor temperature profiles. Mass flow controllers (BROOKS) were used to supply the gases to the reaction cell. The catalysts were pre-treated by heating at 550 °C under O₂. The total flow was 40 ml min⁻¹ in every experiment. A background spectrum series were taken during the cooling down in flowing He to remove any background shift due to temperature and any other temperature effects. Adsorption of a reactant mixture containing [NO] \approx 500 ppm, [CO] \approx 300 ppm, [C₃H₆] \approx 300 ppm, [O₂] \approx 10 vol.% and He as the carrier gas, with the total flow of 40 ml min⁻¹ was performed for 30 min at 150 and 250 °C.

3. Characterization results

3.1. Chemical analysis and N_2 adsorption/desorption

The chemical composition and physico-chemical properties of stabilized and hydrothermally aged catalysts are listed in Table 1.

Table 1. Chemical composition and physical properties of stabilized and HT-aged catalysts.

Samples	Element contents (wt%) ^b						S _{BET} (m ² g ⁻¹) ^d	
	Pt		Pd		Impurity ^c		Stabilized ^a	HT aged
	Stabilized ^a	HT aged	Stabilized ^a	HT aged	Stabilized ^a	HT aged		
PtPd	0.85	0.69	0.49	0.49	-	-	60	38
Na-PtPd	0.83	0.70	0.50	0.50	1.60	0.20	50	31
P-PtPd	0.64	0.54	0.46	0.43	5.60	5.45	33	22

^a Synthesized catalysts before HT-aging.

^b Theoretical element contents (wt%): 0.8% Pt, 0.5% Pd, 2% Na, 7% P. Measurement uncertainty: 3%.

^c Na or P, respectively.

^d BET specific surface area.

ICP results showed a decrease in platinum amount after hydrothermal aged treatment, which could be associated to the leaching of Pt during the HT-aging treatment. The leaching of Na and P species was also evidenced, Table 1, especially in the case of HT-Na-PtPd catalyst. It is worth noting that, although modified catalysts were also stabilized in presence of water, the leaching effect was more pronounced after HT-aging. This effect is probably related to the higher temperature and longer exposition time during HT-aging comparing to the conditions used for stabilized treatment. These results confirmed that the impurities leaching depend of hydrothermal treatment duration. This assumption was corroborated by measuring the pH of the output during the HT-aging process, which became more basic increasing the aging time [22].

The specific surface area (SSA) of HT-aged samples was determined by N_2 adsorption/desorption (Table 1). The obtained values after hydrothermal aging were lower than the SSA found for stabilized catalysts. Otherwise, the isotherms of the HT-aged catalysts were ascribed to type IV isotherms with H3-type of hysteresis, according to the BDDT classification [23]. Although the HT-catalysts still associated with mesoporous materials as the stabilized catalysts, the BJH pore size distribution curves showed that mesopores distribution was mainly centred between 30-50 nm pores size (not shown), which is in agreement with the lower SSA values found for HT-aging catalysts.

The decreases of specific surface area and changes of pores distribution after HT-aging could be attributed to the catalyst sintering. The sintering effect generally takes place at high temperatures and under reaction atmosphere [24]. In particular, water vapour accelerates the crystallization and the structural change in oxide supports. For example, the hydrothermal treatment on alumina supports decreases the surface area and shifts the pore distribution to larger pores [25] due to the closure of the pores occasioned by the elimination of the water on the support. The condensation of hydroxyl groups on alumina surface produced the formation of Al-O-Al bonds, which bring more hydroxyls into adjacency sites and in such way results in the closing of the pores [24]. Additionally, alkali metals, such as Na, affect the thermal properties of the support and can accelerate the sintering process by interaction with acid sites of the alumina [26]. Despite of the lower amount of Na impurity after HT-aging catalysts, the results showed that the presence of alkalis can increase the sintering process, and thus the loss of SSA [27]. Finally, in presence of phosphorus impurities, the SSA also decreased comparing to the reference catalyst, which could probably be ascribed to the pore blocking produced by the formation of phosphates [28].

3.2. X-ray diffraction (XRD)

Figure 1 presents a comparison between the XRD patterns of PtPd, HT-PtPd, HT-Na-PtPd and HT-P-PtPd catalysts, obtained using 2θ positions between 10 and 80°.

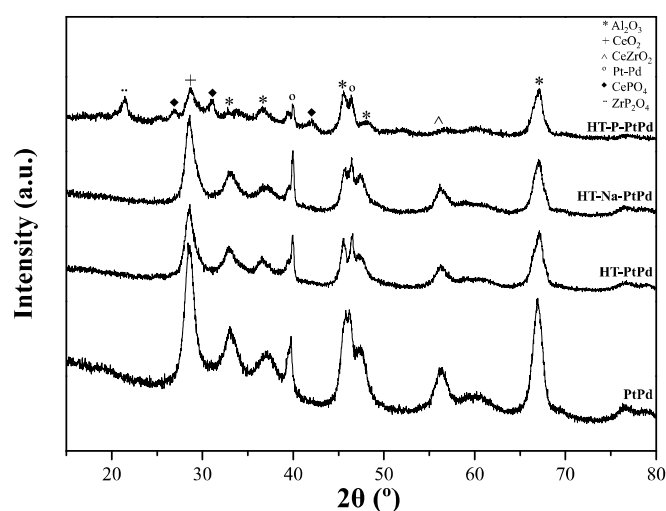


Figure 1. X-ray diffraction patterns of PtPd, HT-PtPd, HT-Na-PtPd and HT-P-PtPd catalysts.

After hydrothermal aging, the peaks at 28.8° and 33.1° corresponding to CeO₂ with cubic structure, and the peak at 56.5° attributed to ceria-zirconia mixed oxide, were still present on the reference HT-PtPd catalyst. In the same way, the peaks related to Al₂O₃ phase at 37° and 67° did not change. However, the peak at 39.5° attributed to alumina, became a shoulder of a more intense peak at 40° in the case of HT-PtPd catalyst. Otherwise, the broad peak centred at 45.8° related to γ -alumina, was divided in two peaks at 45.5° and 46.5° after the hydrothermal aging. The shoulder at 39.5° and peak at 45.5° were related to the alumina phase, while peaks at 40° and 46.5° can be attributed to platinum and/or palladium. The presence of these peaks evidenced the sintering of noble metals after hydrothermal aging for the reference catalyst.

Moreover, the XRD pattern of hydrothermally aged Na-modified catalyst, Figure 1, was similar to that of reference HT-PtPd catalyst. However, the XRD profile of HT-P-PtPd catalyst presented some differences comparing to that of the stabilized catalyst, i.e. same catalyst before HT-aging [8]. Peaks corresponding to CePO₄ (27.1°, 31.2° and 41.9°) and to ZrP₂O₄ (21.5°) were found. The peak at 56.5° attributed to ceria-zirconia mixed oxide was not observed, which could be probably due to the lower amount of Ce and Zr available after the cerium and zirconium phosphates formation.

3.3. Transmission electron microscopy (TEM)

Figure 2 presents the images TEM corresponding to: a) HT-PtPd, b) HT-Na-, and c) HT-P-PtPd catalysts.

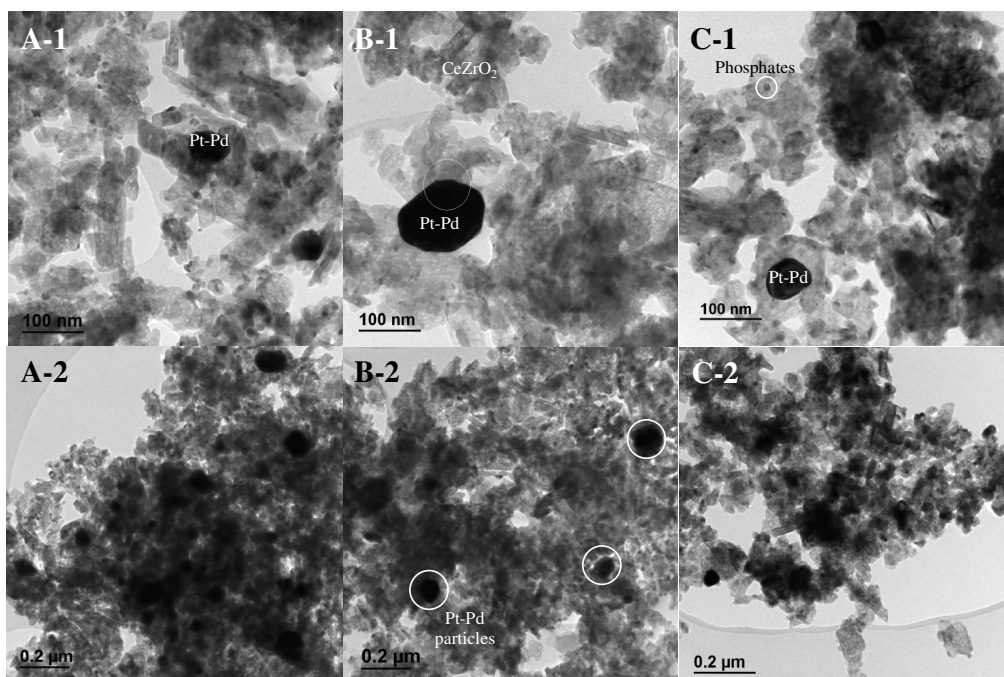


Figure 2. TEM images of the synthesized (scale at images 1 – 100 nm; scale at images 2 – 0.2 μm): A) HT-PtPd, B) HT-Na-PtPd, and C) HT-P-PtPd.

Based on these TEM results, it can be concluded that no significant changes were produced on the alumina-based support after the hydrothermal aging, even in the presence of impurities. This assumption confirms the thermal stabilization of alumina due to the incorporation of lanthanum [29,30]. Ceria-zirconia phase was presented in form of a mixed oxide, well distributed along all the support.

However, the metal particle size of reference PtPd-catalyst was modified after HT-aging comparing to that of the stabilized catalyst analysed in our previous study [8] Figure 2 – A. After HT-aging at 850 $^{\circ}\text{C}$, Pt-Pd particles were now detected by microscopy, which evidenced the sintering of noble metal particles under this treatment, in agreement to the XRD results. Nevertheless, it can be seen that the Pt-Pd particles still well dispersed on this catalyst with an average particle size around 50 nm. Similar results were found for HT-Na-PtPd and HT-P-PtPd catalysts, Figure 2 – B and C. These TEM images lead to appreciate the increase of platinum-palladium particles size and the covering of alumina surface by ceria-zirconia phase as a dispersed phase. In the case of HT-P-PtPd catalyst the formation of dispersed phosphates was also evidenced.

In addition, elemental EDX analysis was performed over all HT-aged catalysts in order to evaluate the presence of different metals. The obtained results indicated that in all the HT-aged catalysts the noble metal particles contained both platinum and

palladium. Nano-diffraction experiments were made on HT-PtPd catalyst in order to identify the crystallographic structure of different noble metals and to verify the formation of an alloy after HT-aging treatment. However, the measured crystallographic structures of Pt, Pd and PtPd were almost similar (0.0390 ± 0.02 nm), thus it was not possible to differentiate the formation of a Pt-Pd alloy accurately.

3.4. X-ray photoelectron spectroscopy (XPS)

Moreover HT-PtPd, HT-Na-PtPd and HT-P-PtPd catalysts, were analysed by XPS in order to evaluate the changes in surface properties after HT-treatment. Firstly, the XPS profiles corresponding to the Al 2p, Figure 3, are centred at the same range (74.6 ± 0.2 eV) for all catalysts, which is associated with γ -Al₂O₃ phase and evidenced that no alumina-phase transition was produced after hydrothermal aging. This peak interferes with most intensive Pt 4f peak, which made impossible to determine the chemical state of platinum.

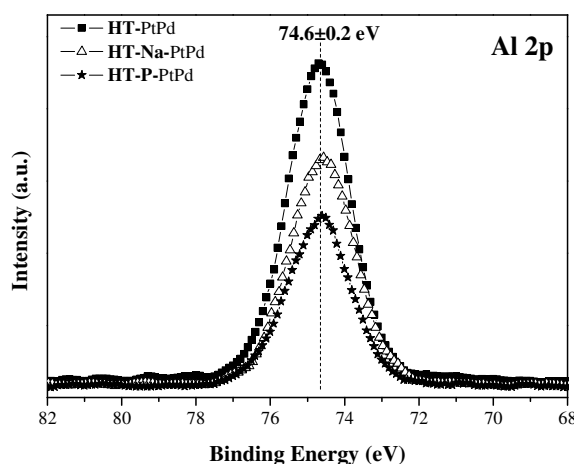


Figure 3. Al 2p XPS spectra of HT-PtPd, HT-Na-PtPd and HT-P-PtPd catalysts.

Figure 4 shows the Ce 3d obtained spectra, in which the peaks characteristics of CeO₂, according to the convention established by Burroughs, are presented for all the catalysts [31,32]. Thus, peaks 1, 3 and 6, 8 and 11 refer to 3d_{3/2} and 3d_{5/2} binding energies, respectively of Ce³⁺ characteristic states, whereas peaks 2, 4, 5 and 7, 9, 10 corresponds to 3d_{3/2} and 3d_{5/2} binding energies of Ce⁴⁺ states. In Table 2 are shown the Ce³⁺/Ce⁴⁺ ratios calculated by decomposition and integration of the corresponding peaks. Reference and Na-modified HT-PtPd catalysts presented similar proportion of Ce³⁺ and Ce⁴⁺ oxidation states, being slightly higher percentage of the oxidized state for the HT-PtPd catalyst (Table 2). However, only the +3 oxidation state of cerium (Ce³⁺) was evidenced for HT-P-PtPd catalyst, which could be attributed to the

presence of phosphorus impurities that stabilize the ceria in its reduced state [33]. This fact confirms that after hydrothermal treatment, the Ce^{3+} species were bounded forming the CePO_4 compound, according to the broad peak depicted at 135.2 ± 0.3 eV corresponding to phosphates, in agreement with the results found by XRD. Moreover, note that binding energy of Pd $3d_{5/2}$ shifted to lower values after HT-aging, Table 2, which could correspond to the formation of Pt-Pd bimetallic phase [34]. Finally, the Na impurities were found at 1072 ± 0.2 eV, with no changes in the chemical state after hydrothermal aging.

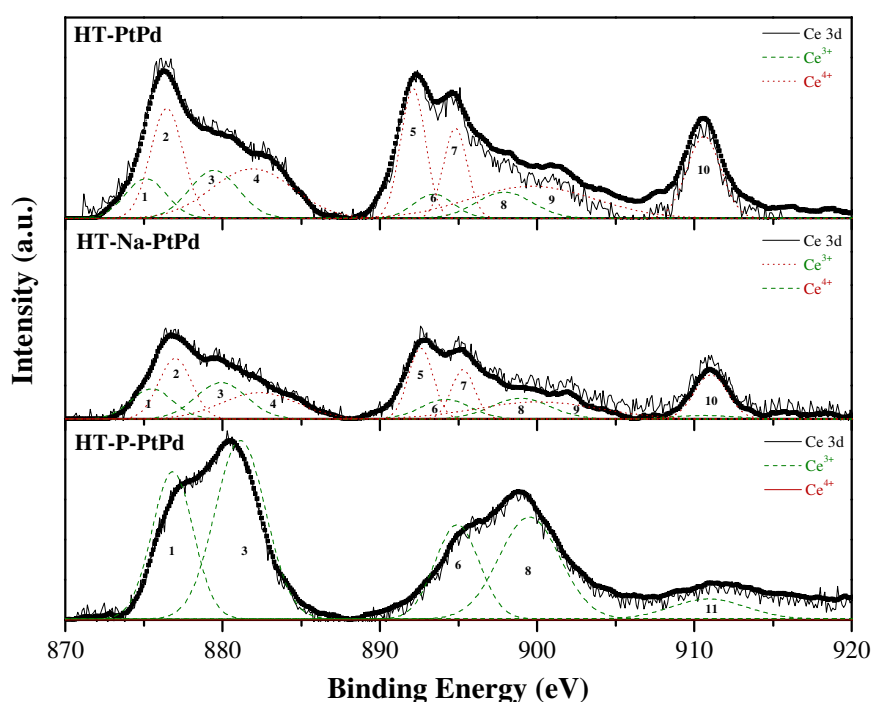


Figure 4. Ce 3d spectra of HT-PtPd, HT-Na-PtPd and HT-P-PtPd catalysts.

Table 2. Binding energies (BEs) of Ce and Pd and percentage of the chemical states of cerium (Ce^{3+} and Ce^{4+}) on the surface obtained from XPS analyses.

Catalyst	PtPd		Na-PtPd		P-PtPd	
	<i>Stabilized</i>	<i>HT-aged</i>	<i>Stabilized</i>	<i>HT-aged</i>	<i>Stabilized</i>	<i>HT-aged</i>
BE						
Ce $3d_{5/2}$ (eV)	884.4	884.2	884.5	884.2	885.0	884.5
BE						
Pd $3d_{5/2}$ (eV)	336.9	332.1	336.7	332.5	336.9	334.5
Ce^{4+} (%)	58.5%	88.0%	52.9%	84.2%	45.7%	0.0%
Ce^{3+} (%)	41.5%	12.0%	47.1%	15.8%	54.3%	100%

3.5. H₂ temperature programmed reduction (H₂-TPR)

In order to analyse the influence of hydrothermal aging on the reducibility of the catalysts, H₂ temperature programmed reduction experiments were carried out from room temperature to 650 °C. A comparison between the TPR profiles of stabilized and HT-aged PtPd, Na-PtPd and P-PtPd catalysts is shown in Figure 5.

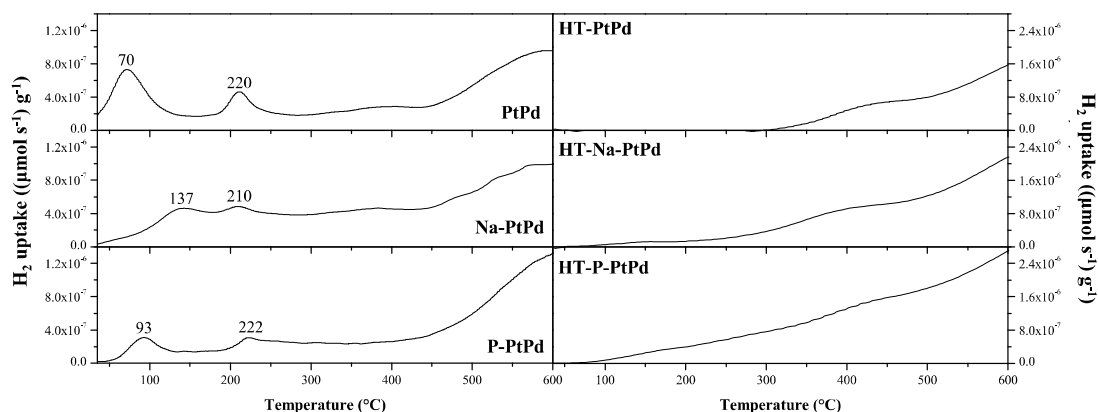


Figure 5. TPR-H₂ profiles of stabilized PtPd, Na-PtPd and P-PtPd catalysts (left), and HT-PtPd, HT-Na-PtPd and HT-P-PtPd catalysts (right).

In our previous study we have verified the presence of two reduction peaks: one corresponding to the reduction of PdO species around 70 °C for the stabilized PtPd catalyst; and another one observed at 220 °C attributed to the reduction of PtO_x species [8]. Finally, the broad peak at temperatures higher than 450 °C was associated with the reduction of bulk ceria promoted by zirconium [35,36].

Notwithstanding, the reduction profiles of HT-aged catalysts only presented a small broad peak between 350 – 450 °C, which could be attributed to the reduction of superficial CeO₂ that is not interacting with metal. This is in agreement with the decrease of SSA due to the catalyst sintering that would reduce the metal-ceria interaction [37]. In addition, the HT-aging treatment could produce a deterioration of the surface oxygen mobility capacity increasing the reduction temperature [38]. Thus, the reducibility of the support would decrease, increasing the percentage of ceria reduced at higher temperatures than in the case of stabilized catalysts. It is worth noting that after HT-aging treatment no peaks corresponding to the reduction of palladium and platinum were evidenced. Previous characterization results of HT-aged catalysts (XRD, TEM) have proved the sintering of Pt-Pd particles produced after HT-aging. Thus, the decrease of reducibility could be ascribed to the formation of Pt-Pd bimetallic particles. Previous studies [18,19] also found a lower H₂ consumption

for aged bimetallic catalysts. In agreement with the discussed results, they considered that the metal sintering would limit the re-oxidation of the catalysts, thus decreasing the subsequent reduction. The presence of cerium near to the noble metal particles on the catalyst surface may facilitate the charge transfer from Pt-Pd to Ce support, resulting in higher noble metal oxidation state [37]. However, the sintering of the catalyst decreased the metal-support interaction, inhibiting the effect of cerium on the noble metal phase.

4. Activity test results

The reaction rates of CO, C₃H₆ and NO for hydrothermally aged catalysts at conversions lower than 10% are shown in Table 3. A comparison with stabilized catalysts data was done in order to evaluate the influence of the HT-aging process in presence of impurities.

Table 3. Catalytic activity results obtained with stabilized and HT-aged PtPd, Na-PtPd and P-PtPd catalysts for catalytic diesel oxidation reaction.

Catalyst	¹ r _{CO} (150°C)		¹ r _{C₃H₆} (180°C)		¹ r _{NO} (230°C)	
	<i>Stabilized</i>	<i>HT-Aged</i>	<i>Stabilized</i>	<i>HT-Aged</i>	<i>Stabilized</i>	<i>HT-Aged</i>
PtPd	0.912	0.081	-	0.075	3.191	1.893
Na-PtPd	0.421	0.084	0.045	0.033	0.736	-
P - PtPd	0.994	0.256	0.446	0.144	3.643	-

¹Reaction rate ((mol s⁻¹ g_{PGM}⁻¹)·10⁵) during the heating at 150, 180 and 230 °C for CO, C₃H₆ and NO, respectively for the first catalytic cycle.

To begin with, HT-aged catalysts presented in general lower CO reaction rate than stabilized ones. After HT-aging, the redox capacities of ceria were diminished, as verified by H₂-TPR [39]. This would decrease the oxygen activation on the catalyst and subsequently the reaction rate of CO (Table 3) related to its “self-poisoning” effect [37]. Until the temperature was not high enough to CO could desorb, the oxygen would not be available to initiate the reaction. Nevertheless, comparing all HT-aged catalysts, higher reaction rate values for CO at 150 °C were found in presence of Na and P impurities (Table 3). The low electronegativity of Na impurities produces an inhomogeneous electric field that promotes the adsorption of CO. However, relating with the catalyst sintering, this electronic effect would be inhibited and lower metal-CO charge transfer would be produced [40]. Consequently the saturation of the catalyst surface produced by CO adsorption was avoided, increasing slightly the reaction rate for HT-Na-PtPd catalyst. Finally, the presence of phosphates

verified by physico-chemical characterizations, also produced the inhibition of CO catalyst saturation for HT-P-PtPd catalyst, increasing the reaction rate.

Secondly, the C₃H₆ reaction rate calculated at 180 °C, presented lower values for HT-aged catalysts than the stabilized ones due to their lower redox capacity. In the case of HT-PtPd, the obtained C₃H₆ reaction rate was higher than for stabilized-PtPd catalyst. This higher value could be probably due to the promotion of NO reduction to N₂O via C₃H₆-SCR. Previous studies [41] have shown that the higher size of bimetallic particles enhances NO reduction to N₂O. Thus, the sintering of Pt-Pd particles after HT-aging would increase the C₃H₆ reaction rate. However, comparing with HT-PtPd catalyst, the presence of Na impurities decreased the reaction rate, while higher value was found for HT-P-PtPd catalyst. As discussed above, due to the catalyst sintering the promotion effect of the Na impurities was decreased. The induced strengthening of electron-accepting adsorbates such as O₂ produced by the electron donor behaviour of Na impurities would be inhibited. Consequently the O₂ adsorption will be disfavored, decreasing the C₃H₆ conversion [6]. Similarly to the obtained results with CO, the formation of phosphates would also avoid the propylene adsorption, inhibiting its self-poisoning.

Finally, the reaction rate of NO at 230 °C was also lower after HT-aging comparing to that of the stabilized catalysts. This could be associated to the active sites amount decreased due the noble metal sintering. Otherwise, the promoted NO adsorption by alkali impurities was suppressed due to the leaching of Na and the sintering of the catalyst [6,42]. In the case of HT-P-PtPd, the blockage of catalytic active sites by the higher amount of phosphates and the formation of phosphates oxides decreased the NO reaction rate.

5. In-situ DRIFTS study

Once the influence of HT-aging on physico-chemical, redox and catalytic activity of reference and modified-catalysts was verified, direct spectroscopy evidenced by in-situ Diffuse Reflectance Infrared Fourier Transform Spectroscopy (DRIFTS) were performed by exposition to a NO + CO + C₃H₆ + O₂ gas mixture at 150 °C and 250 °C respectively. The principal bands observed and the corresponding assignments are summarized in Table 4.

Table 4. Bands position and the corresponding assignments of surface species in DRIFT spectra.

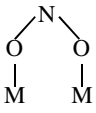
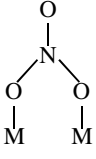
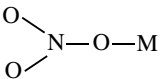
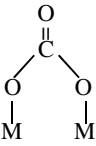
Surface species	Peak position (cm ⁻¹)	Infrared vibration	Reference	
Bridging nitrites 	1314-1266	$\nu_{as}(\text{NO}_2)$	[42]	
	1230-1276	$\nu_s(\text{NO}_2)$		
Bridging nitrates 	1600-1650	$\nu_s(\text{NO}_2)$	[43-45]	
	1200-300	$\nu_{as}(\text{NO}_2)$		
Monodentate nitrates 	1510-1508	$\nu_{as}(\text{NO}_2)$	[46]	
	1275-1250	$\nu_s(\text{NO}_2)$		
Linear or bent NO on Pt	(NO) ⁻	1680-1780	$\nu(\text{N-O})$	[42,47]
Formates	(HCOO) ⁻	1373	$\nu_s(\text{COO}^-)$	[48-51]
		1410-1390	$\delta(\text{CH})$	
		1585	$\nu_{as}(\text{COO}^-)$	
Acetates	(CH ₃ -(C=O)-O) ⁻	1460-1440	$\nu_s(\text{COO}^-)$	[51,52]
		1555-1545	$\nu_{as}(\text{COO}^-)$	
		1645	$\nu_{as}(\text{COO}^-)$	
Carbonates		1350-1345	$\nu_s(\text{COO}^-)$	[51,52]

Figure 6 depicts the evolution of IR spectra of adsorbed species on the surface of PtPd (up) and HT-PtPd (down) catalysts under NO + CO + C₃H₆ + O₂ gas mixture at 150 °C.

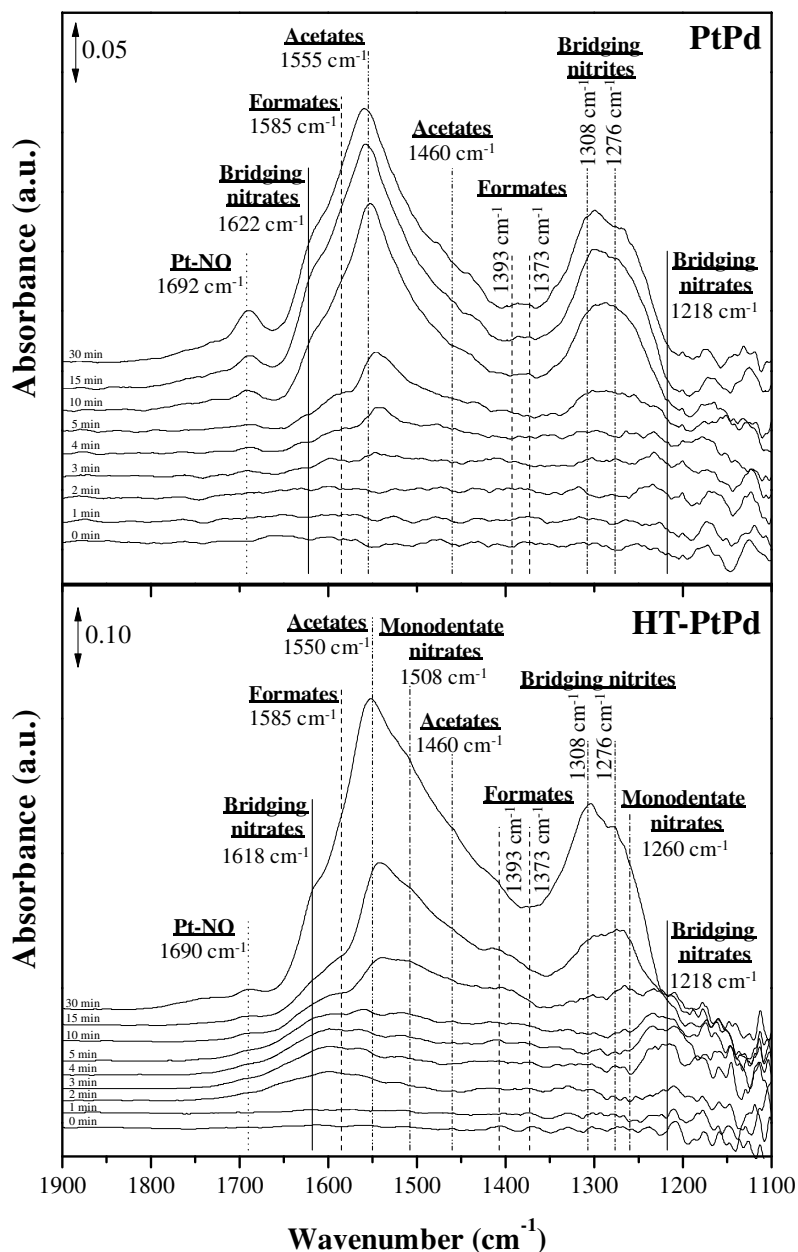


Figure 6. DRIFT spectra in the region 1900-1100 cm^{-1} of PtPd (up) and HT-PtPd (down) catalysts at 150 $^{\circ}\text{C}$ under simulated exhaust conditions. FT-IR chamber feed: $[\text{NO}] \approx 500$ ppm, $[\text{CO}] \approx 300$ ppm, $[\text{C}_3\text{H}_6] \approx 300$ ppm, $[\text{O}_2] \approx 10$ vol.%, He as balance. Total flow: 40 ml min^{-1} .

The bands mainly found for PtPd reference catalyst (Fig. 6 up) were associated with nitroxy species, corresponded to bridging nitrites (1308 cm^{-1} , $\nu_{\text{as}}(\text{NO}_2)$; 1276 cm^{-1} , $\nu_{\text{s}}(\text{NO}_2)$) and bridging nitrates (shoulder at 1622 cm^{-1} , $\nu_{\text{s}}(\text{NO}_2)$; 1218 cm^{-1} , $\nu_{\text{as}}(\text{NO}_2)$). Moreover, acetates (1555 cm^{-1} , $\nu_{\text{as}}(\text{COO}^-)$; 1460 cm^{-1} , $\nu_{\text{s}}(\text{COO}^-)$) and formates (1585 cm^{-1} , $\nu_{\text{as}}(\text{COO}^-)$; 1393 cm^{-1} , $\delta(\text{CH})$; 1373 cm^{-1} , $\nu_{\text{s}}(\text{COO}^-)$) were also

observed, corresponding to reaction intermediates of CO and C₃H₆ oxidation reactions [48,49]. In addition, a band at 1692 cm⁻¹ corresponding to N – O stretch of linear or bent molecular NO species adsorbed on Pt ($\nu(\text{N-O})$) was depicted in PtPd spectra. Regarding the evolution of the bands increasing the time, formates and acetates species were firstly formed. The previous reaction rates values showed that CO and C₃H₆ oxidations started at lower temperatures than NO consumption because they are strongly adsorb on the catalyst surface. Thus, it seems evident that the catalyst surface will be saturated by reactions intermediates, in agreement with the higher intensities of peaks corresponding to carbonaceous species. Nevertheless, NO adsorption also occurred, according to the formation of bridging nitrites and nitrates. Moreover, the interaction of NO with metal Pt particles was shown by the appearance of a band at 1692 cm⁻¹. This could be attributed to the reduction of the metal during CO and C₃H₆ oxidations, freeing active sites for NO adsorption.

After HT-aging (HT-PtPd catalyst, Fig. 6 down), the bridging nitrates were the first species observed on the catalyst surface and new bands related to monodentate nitrates (1508 cm⁻¹, $\nu_{\text{as}}(\text{NO}_2)$; 1260 cm⁻¹, $\nu_{\text{s}}(\text{NO}_2)$) were observed. It is worth noting that the intensity of bridging nitrites bands is higher than more stable nitrates species.

It seems that because of their high oxidant character, adsorbed nitrates oxidize C₃H₆ while they were reduced to nitrites. This conclusion is in agreement with the higher C₃H₆ reaction rate obtained for HT-PtPd comparing to that of stabilized-PtPd catalyst (Table 3), which was previously associated to NO reduction to N₂O via HC-SCR. Additionally, previous studies have shown that Pd exhibits strong structure sensitivity for NO adsorption [53]. Thus, the higher Pt-Pd particles size after HT-aging could enhance NO dissociative chemisorption.

Moreover, IR spectra of adsorbed species on the surface of Na-PtPd and HT-Na-PtPd catalysts under the same conditions are shown in Figure 7.

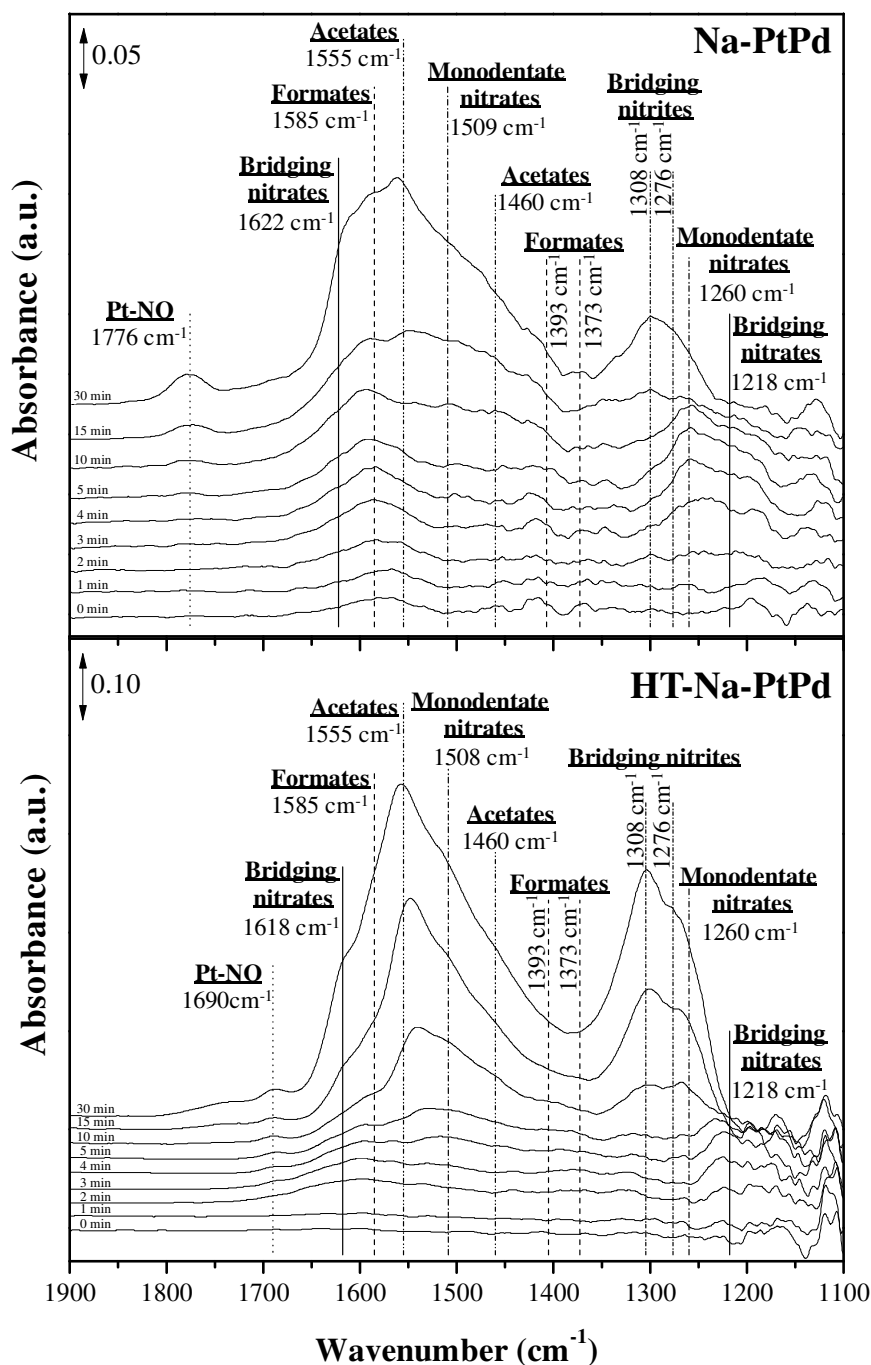


Figure 7. DRIFT spectra in the region 1900-1100 cm^{-1} of Na-PtPd (up) and HT-Na-PtPd (down) catalysts at 150 °C under simulated exhaust conditions. FT-IR chamber feed: $[\text{NO}] \approx 500$ ppm, $[\text{CO}] \approx 300$ ppm, $[\text{C}_3\text{H}_6] \approx 300$ ppm, $[\text{O}_2] \approx 10$ vol.%, He as balance. Total flow: 40 ml min^{-1} .

Similarly to the DRIFT spectra of stabilized-PtPd catalyst, in presence of Na impurities, formates (1585 cm^{-1} , $\nu_{\text{as}}(\text{COO}^-)$), 1393 cm^{-1} , $\delta(\text{CH})$, 1373 cm^{-1} , $\nu_{\text{s}}(\text{COO}^-)$) and acetates (1555 cm^{-1} , $\nu_{\text{as}}(\text{COO}^-)$, 1455 cm^{-1} , $\nu_{\text{s}}(\text{COO}^-)$) were the first adsorbed species to depict. In addition, increasing the exposition time, bridging nitrites (1308

cm^{-1} , $\nu_{\text{as}}(\text{NO}_2)$; 1276 cm^{-1} , $\nu_{\text{s}}(\text{NO}_2)$), bridging nitrates (1618 cm^{-1} , $\nu_{\text{s}}(\text{NO}_2)$; 1218 cm^{-1} , $\nu_{\text{as}}(\text{NO}_2)$) and monodentate nitrates (1508 cm^{-1} , $\nu_{\text{as}}(\text{NO}_2)$; 1260 cm^{-1} , $\nu_{\text{s}}(\text{NO}_2)$) were evidenced. The band corresponding to the stretch of linear or bent NO adsorbed species on Pt phase was also present at 1776 cm^{-1} . Comparing to the stabilized-PtPd catalyst profile (Fig. 6 up), the Na-PtPd spectra (Fig. 7 up) presented more pronounced intensities bands. As previously discussed, the electro-donor behaviour of alkali metals such as Na, increases the metal-NO (and/or CO) interaction [5]. Thus, the NO and/or CO adsorption would be favored, in agreement with the more pronounced peak in presence of Na at the saturation moment.

When the catalyst was HT-aged (Fig. 7, down), the adsorption trend was similar to that of the reference HT-PtPd catalyst. Only slightly higher intensity of the bands associated with bridging nitrites was detected in the case of HT-Na-PtPd comparing to that of the HT-PtPd catalyst. In agreement with the similar bands observed by in-situ DRIFTS, alkali effects were attenuated after HT-aging. This could be ascribed to two facts: (i) the leaching of alkali impurities during HT-aging, and (ii) the lower alkali-metal phase interaction [6], which could decrease their electronic effect on catalytic activity.

Finally, phosphorus-modified catalyst was compared with HT-P-PtPd catalyst spectra in Figure 8.

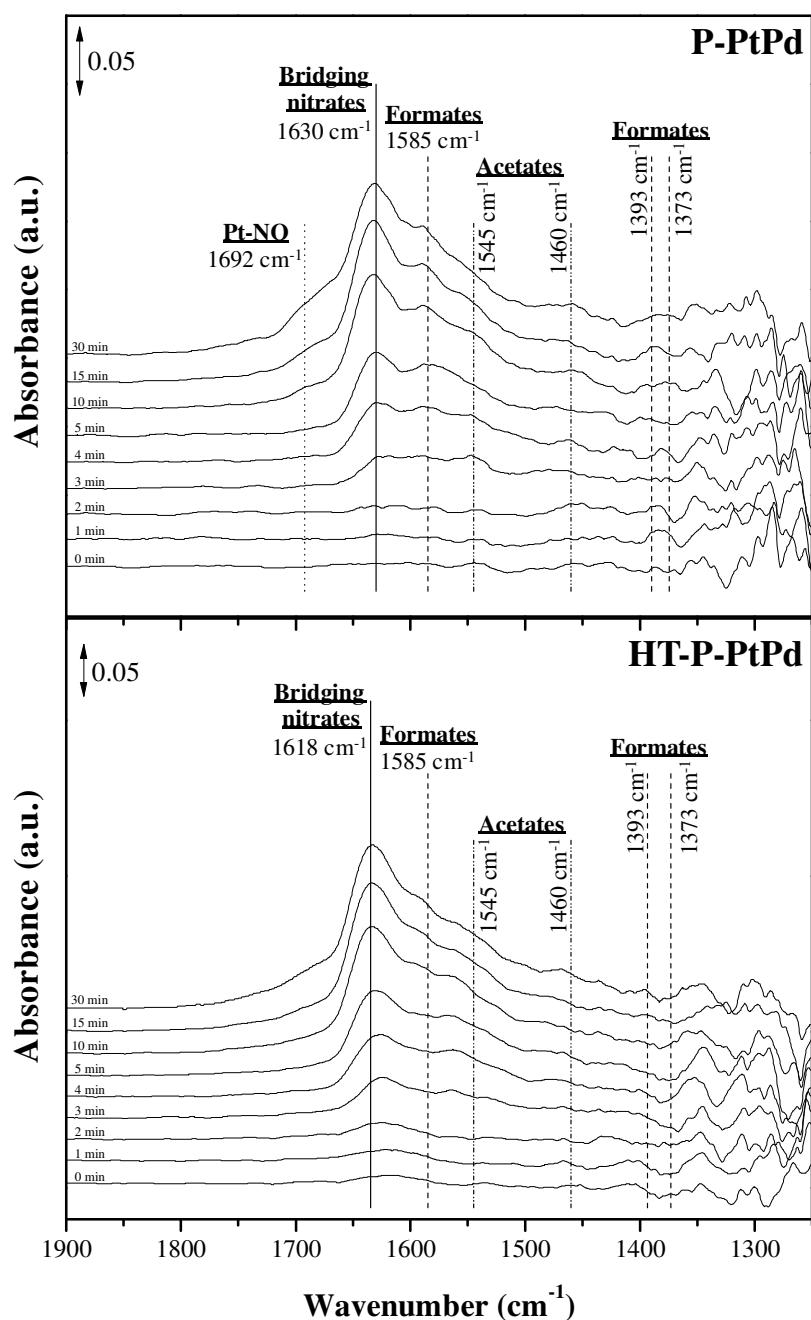


Figure 8. DRIFT spectra in the region 1900-1100 cm^{-1} of P-PtPd (up) and HT-P-PtPd (down) catalysts at 150 $^{\circ}\text{C}$ under simulated exhaust conditions. FT-IR chamber feed: $[\text{NO}] \approx 500$ ppm, $[\text{CO}] \approx 300$ ppm, $[\text{C}_3\text{H}_6] \approx 300$ ppm, $[\text{O}_2] \approx 10$ vol.%, He as balance. Total flow: 40 ml min^{-1} .

In both cases, stabilized P-PtPd and HT-P-PtPd catalysts, only bridging nitrates at 1630 cm^{-1} ($\nu_s(\text{NO}_2)$) and 1618 cm^{-1} ($\nu_s(\text{NO}_2)$) were detected as principal adsorbed species. Moreover, broad peaks corresponding to formates (1585 cm^{-1} , $\nu_{\text{as}}(\text{COO}^-)$; 1393 cm^{-1} , $\delta(\text{CH})$; 1373 cm^{-1} , $\nu_s(\text{COO}^-)$) and acetates (1545 cm^{-1} , $\nu_{\text{as}}(\text{COO}^-)$; 1460

cm^{-1} , $\nu_s(\text{COO}^-)$) were observed. However, their intensities were negligible comparing to that of reference PtPd-catalysts, even after HT-aging. The weak adsorption in presence of phosphorus could be attributed to the formation of phosphates, which would block the adsorption sites. Moreover, the adsorption of NO instead of CO and/or C_3H_6 could be attributed to the presence of Ce^{3+} species, according to XPS results, which promotes NO decomposition [54]. This low adsorption could explain the higher reaction rates found for P-modified catalysts. The blockage of adsorption sites favored the CO and C_3H_6 oxidation and direct desorption to the gas-phase, avoiding the saturation of the catalyst surface. For NO, however, the reaction rate was lower than that of the reference HT-PtPd catalyst. Regarding the obtained spectra, no peak related to the interaction NO-Pt after HT-aging. Thus, the lower NO reaction rate could be ascribed to the blocking of active sites by the higher phosphates formation verified by TEM and XRD.

Finally, the temperature was increased up to 250 °C under exposition to the same gas mixture. The Figure 9 shows the DRIFTS spectra obtained for stabilized and HT-aging catalysts. Particularly, Figure 9-A shows the comparison between PtPd and HT-PtPd catalysts at the saturation at 250 °C, in which was evidenced the lower adsorption over stabilized-PtPd catalyst than HT-aged PtPd catalyst. It seems evident that after HT-aging, the oxidation reactions shifted towards higher temperatures. Thus, the catalyst surface was still saturated of un-reacted reaction intermediates such as formates, acetates and nitrites. The presence of carbonates bands (1645 cm^{-1} , $\nu_{\text{as}}(\text{COO}^-)$; 1350 cm^{-1} , $\nu_s(\text{COO}^-)$) were also evidenced after HT-aging, coming from the adsorption of CO_2 produced during CO and C_3H_6 oxidations. Higher intensity of carbonates bands on the HT-PtPd catalyst spectrum was also evidenced due to the blockage of the active sites, delaying the NO oxidation as verified by the lower NO reaction rate obtained after HT-aging (Table 2).

In presence of Na impurities (Figure 9-B) some differences were observed. The spectrum of Na-PtPd catalyst presented weak carbonaceous species adsorption. Nevertheless, nitrites and nitrates species still presented as well as the broad peak at 1776 cm^{-1} associated with the Pt-NO interaction. As previously discussed, the low electronegativity of Na impurities promotes the metal-NO interaction, which would increase the NO adsorption and subsequently decreased its reaction rate (Table 3). After HT-aging, similar conclusions than that of the HT-PtPd catalyst were found. It is worth noting the higher intensity of carbonates bands, which could due to the

higher basicity of Na that would increase the CO₂ adsorption. Finally, P-PtPd and HT-PtPd catalysts (Figure 9-C) presented slightly NO adsorption in form of nitrates, with a shoulder corresponding to carbonates species. It seems that the active sites still blocked by phosphates formation at 250 °C, avoiding NO oxidation.

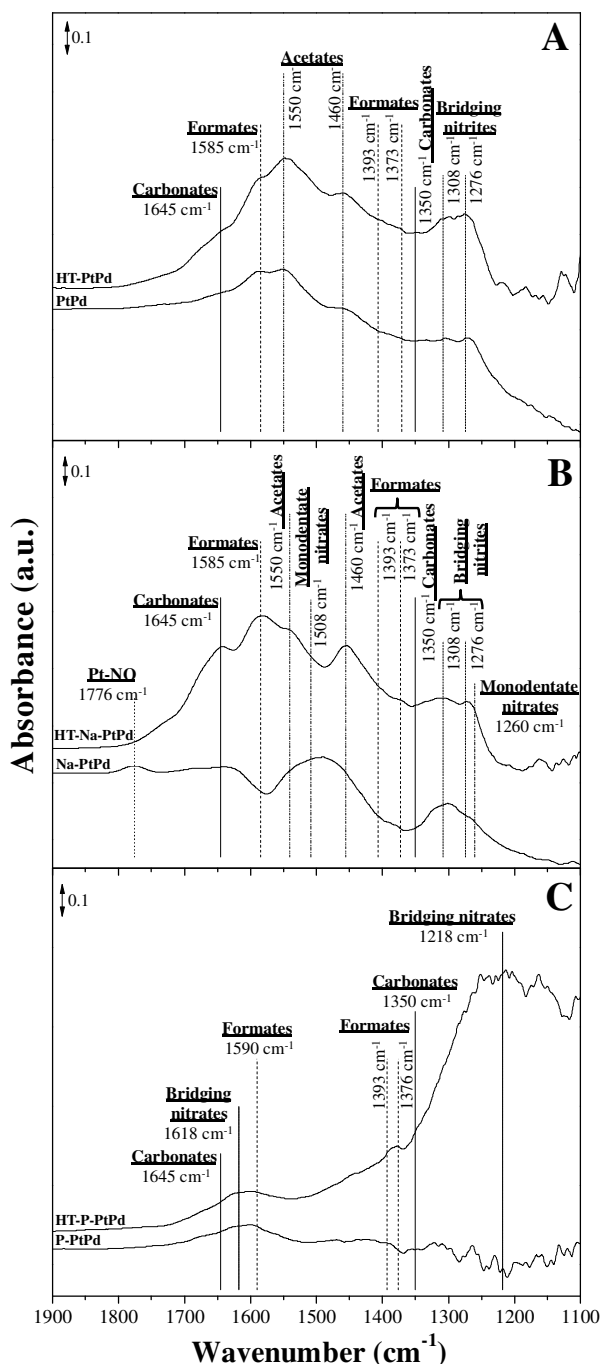


Figure 9. DRIFT spectra in the region 1900-1100 cm⁻¹ of stabilized and HT-aged PtPd (A), Na-PtPd (B) and P-PtPd (C) catalysts at 250 °C under simulated exhaust conditions. FT-IR chamber feed: [NO] ≈ 500 ppm, [CO] ≈ 300 ppm, [C₃H₆] ≈ 300 ppm, [O₂] ≈ 10 vol.%, He as balance. Total flow: 40 ml min⁻¹.

6. Conclusions

The hydrothermal aging impact on the physico-chemical, redox and catalytic activity of PtPd/CeZrO₂/La-Al₂O₃ diesel oxidation catalyst modified with Na and P species was investigated. The physico-chemical characterization results showed the sintering of the catalyst and the higher Pt-Pd bimetallic particles size, which lowered the number of catalytic active sites. The redox capacities of HT-aged catalysts were also decreased, according to the H₂-TPR results, inhibiting the oxidation reactions. In agreement with these conclusions, lower reaction rates were found for CO, C₃H₆ and NO involved reactions after HT-aging treatment of catalyst. The infrared spectra indicated the promoted adsorption of NO after HT-aging, related to the higher Pt-Pd particles size. The leaching of alkali impurities, as well as the catalyst sintering, was also evidenced, which weakened the promoted adsorption of electron-accepting adsorbates, such as CO, NO and O₂. Thus, although it had a positive effect on the CO oxidation due to the inhibition of the “self-inhibition” effect, it decreased the reaction rates of C₃H₆ and NO. Finally, the formation of phosphates species on HT-aged P-modified-PdPt catalyst was evidenced by XRD and TEM analyses. As verified by in-situ DRIFTS experiments, it inhibited the catalyst surface saturation, increasing CO and C₃H₆ reaction rates. However, NO oxidation was disfavored due to the blockage of catalytic active sites by the formed phosphates.

Acknowledgements

The authors gratefully acknowledge the University Claude Bernard Lyon 1, the National Center for Scientific Research (CNRS) and the French National Agency of Research for its financial support (Appibio Project, Ref. ANR-14-CE22-0003). The authors would like to thank the scientific service of IRCELYON for the assistance in catalytic and physico-chemical characterizations and for stimulating discussions.

References

- [1] M. Adamowska, V. Lauga, P. Da Costa, *Top. Catal.* 56 (2013) 267–272.
- [2] A.P. Wong, E.A. Kyriakidou, T.J. Toops, J.R. Regalbuto, *Catal. Today* 267 (2016) 145–156.
- [3] H. Zhang, S. Yuan, J.L. Wang, M.C. Gong, Y. Chen, *Chem. Eng. J.* 327 (2017) 1066–1076.
- [4] H. Xu, Y. Li, B. Xu, Y. Cao, X. Feng, M. Sun, M. Gong, Y. Chen, *J. Ind. Eng. Chem.* 36 (2016) 334–345.
- [5] M. Konsolakis, N. Macleod, J. Isaac, I. V. Yentekakis, R.M. Lambert, *J. Catal.* 193 (2000) 330–337.
- [6] I. V. Yentekakis, V. Tellou, G. Botzolaki, I.A. Rapakousios, *Appl. Catal. B Environ.* 56 (2005) 229–239.
- [7] I. V. Yentekakis, M. Konsolakis, R.M. Lambert, N. MacLeod, L. Nalbantian, *Appl. Catal. B Environ.* 22 (1999) 123–133.
- [8] P. Anguita, J.M. García-Vargas, F. Gaillard, E. Iojoiu, S. Gil, A. Giroir-Fendler, *Chem. Eng. J.* 352 (2018) 333–342.
- [9] J. Andersson, M. Antonsson, L. Eurenus, E. Olsson, M. Skoglundh, *Appl. Catal. B Environ.* 72 (2007) 71–81.
- [10] M. Kärkkäinen, T. Kolli, M. Honkanen, O. Heikkinen, M. Huuhtanen, K. Kallinen, T. Lepistö, J. Lahtinen, M. Vippola, R.L. Keiski, *Top. Catal.* 58 (2015) 961–970.
- [11] Y. Liang, C. Ou, H. Zhang, X. Ding, M. Zhao, J. Wang, Y. Chen, *Ind. Eng. Chem. Res.* 57 (2018) 3887–3897.
- [12] H. Xiong, E. Peterson, G. Qi, A.K. Datye, *Catal. Today* 272 (2016) 80–86.
- [13] B.B. Hansen, A.D. Jensen, P.A. Jensen, *Fuel* 106 (2013) 234–240.
- [14] A. Morlang, U. Neuhausen, K. V. Klementiev, F.W. Schütze, G. Mieke, H. Fuess, E.S. Lox, *Appl. Catal. B Environ.* 60 (2005) 191–199.

- [15] M. Kaneeda, H. Iizuka, T. Hiratsuka, N. Shinotsuka, M. Arai, *Appl. Catal. B Environ.* 90 (2009) 564–569.
- [16] J.M. Herreros, S.S. Gill, I. Lefort, A. Tsolakis, P. Millington, E. Moss, *Appl. Catal. B Environ.* 147 (2014) 835–841.
- [17] M. Chen, L.D. Schmidt, *J. Catal.* 56 (1979) 198–218.
- [18] E. Rogemond, R. Fréty, V. Perrichon, M. Primet, M. Chevrier, C. Gauthier, F. Mathis, *Appl. Catal. A Gen.* 156 (1997) 253–265.
- [19] X. Auvray, L. Olsson, *Appl. Catal. B Environ.* 168–169 (2015) 342–352.
- [20] C. Bartholomew, *Catal. Today* 212 (2001) 17–60.
- [21] T. Kanerva, V. Kröger, K. Rahkamaa-Tolonen, M. Vippola, T. Lepistö, R.L. Keiski, *Top. Catal.* 45 (2007) 137–142.
- [22] B.C. Bunker, G.W. Arnold, E.K. Beauchamp, D.E. Day, *J. Non. Cryst. Solids* 58 (1983) 295–322.
- [23] G. Leofanti, M. Padovan, G. Tozzola, B. Venturelli, *Catal. Today* 41 (1998) 207–219.
- [24] A. Kalantar Neyestanaki, F. Klingstedt, T. Salmi, D.Y. Murzin, *Fuel* 83 (2004) 395–408.
- [25] M. Skoglundh, L.O. Löwendahl, J.E. Otterated, *Appl. Catal.* 77 (1991) 9–20.
- [26] C.H. Bartholomew, *Appl. Catal. A Gen.* 212 (2001) 17–60.
- [27] S.R. de Miguel, O.A. Scelza, A.A. Castro, J. Soria, *Top. Catal.* 1 (1994) 87–94.
- [28] V. Kröger, M. Hietikko, U. Lassi, J. Ahola, K. Kallinen, R. Laitinen, R.L. Keiski, *Top. Catal.* 30–31 (2004) 469–474.
- [29] B. Béguin, E. Garbowski, M. Primet, *Appl. Catal.* 75 (1991) 119–132.
- [30] X. Chen, Y. Liu, G. Niu, Z. Yang, M. Bian, A. He, *Appl. Catal. A Gen.* 205 (2001) 159–172.
- [31] A. Pfau, K.-D. Schierbaum, *Surf. Sci.* 6028 (1994).
- [32] J.C.S. Dalton, B.P. Burroughs, A. Hamnett, A.F. Orchard, G. Thornton, (1975).
- [33] C. Battistoni, V. Cantelli, M. Debenedetti, S. Kačiulis, G. Mattogno, A. Napoli, *Appl. Surf. Sci.* 144–145 (1999) 390–394.

- [34] Q. Yuan, Z. Zhou, J. Zhuang, X. Wang, *Chem. Commun.* 46 (2010) 1491–1493.
- [35] S. Ricote, G. Jacobs, M. Milling, Y. Ji, P.M. Patterson, B.H. Davis, *Appl. Catal. A Gen.* 303 (2006) 35–47.
- [36] H.-W. Jen, G. Graham, W. Chun, R. McCabe, J.-P. Cuif, S. Deutsch, O. Touret, *Catal. Today* 50 (1999) 309–328.
- [37] Y. Yu Yao, *J. Catal.* 87 (1984) 152–162.
- [38] J. Gong, D. Wang, J. Li, K. Kamasamudram, N. Currier, A. Yezerets, *Catal. Today* (2018) 0–1.
- [39] J.R. González-velasco, J.A. Botas, R. Ferret, M.P. González-marcos, J. Marc, M.A. Gutiérrez-ortiz, 59 (2000) 395–402.
- [40] N.D. Lang, S. Holloway, J.K. Nørskov, *Surf. Sci.* 150 (1985) 24–38.
- [41] J.M. García-Cortés, J. Pérez-Ramírez, J.N. Rouzaud, A.R. Vaccaro, M.J. Illán-Gómez, C. Salinas-Martínez De Lecea, *J. Catal.* 218 (2003) 111–122.
- [42] S. Koukiou, M. Konsolakis, R.M. Lambert, I. V. Yentekakis, *Appl. Catal. B Environ.* 76 (2007) 101–106.
- [43] K.I. Hadjiivanov, *Catal. Rev. Sci. Eng.* 42 (2000) 71–144.
- [44] B. Westerberg, E. Fridell, *J. Mol. Catal. A Chem.* 165 (2001) 249–263.
- [45] A. Kotsifa, D.I. Kondarides, X.E. Verykios, *Appl. Catal. B Environ.* 72 (2007) 136–148.
- [46] J.Y. Luo, W.S. Epling, G. Qi, W. Li, *Catal. Letters* 142 (2012) 946–958.
- [47] A. Bourane, O. Dulaurent, S. Salasc, C. Sarda, C. Bouly, D. Bianchi, *J. Catal.* 204 (2001) 77–88.
- [48] W. Schießer, H. Vinek, A. Jentys, *Appl. Catal.* 33 (2001) 263–274.
- [49] M. Haneda, N. Bion, M. Daturi, J. Saussey, J.C. Lavalley, D. Duprez, H. Hamada, *J. Catal.* 206 (2002) 114–124.
- [50] K. Shimizu, H. Kawabata, A. Satsuma, T. Hattori, *J. Phys. Chem. B* 103 (1999) 5240–5245.
- [51] V. Matsouka, M. Konsolakis, R.M. Lambert, I. V. Yentekakis, *Appl. Catal. B Environ.*

- 84 (2008) 715–722.
- [52] K. ichi Shimizu, J. Shibata, H. Yoshida, A. Satsuma, T. Hattori, *Appl. Catal. B Environ.* 30 (2001) 151–162.
- [53] P.W. Davies, R.M. Lambert, *Surf. Sci.* 110 (1981) 227–249.
- [54] C.A. Franchini, D. V. Cesar, M. Schmal, *Catal. Letters* 137 (2010) 45–54.

Absorbance (a.u.)

